MOLECULAR AND CELLULAR BIOLOGY, Apr. 2010, p. 1703–1717 Vol. 30, No. 7
0270-7306/10/$12.00 doi:10.1128/MCB.01226-09

The Motor Protein Myosin-X Transports VE-Cadherin along Filopodia To Allow the Formation of Early Endothelial Cell-Cell Contacts▽†

Sébastien Almagro,[1,2,3]‡ Claire Durmort,[3,4]‡ Adeline Chervin-Pétinot,[1,2,3]‡ Stephanie Heyraud,[1,2,3,4]‡ Mathilde Dubois,[6]‡ Olivier Lambert,[6]‡ Camille Maillefaud,[3,4] Elizabeth Hewat,[5]‡ Jean Patrick Schaal,[7]‡ Philippe Huber,[1,2,3]‡ and Danielle Gulino-Debrac[1,2,3]‡*

Laboratoire de Physiopathologie Vasculaire, CEA, 38054 Grenoble, France[1]; INSERM U882, 38054 Grenoble, France[2]; Université Joseph Fourier, Grenoble, France[3]; Laboratoire d'Ingénierie des Macromolécules[4] and Laboratoire de Microscopie Electronique Structurale,[5] Institut de Biologie Structurale Jean-Pierre Ebel UMR CNRS 5075, Grenoble, France; CBMN UMR CNRS 5248-Institut Européen de Chimie et de Biologie, Université Bordeaux 1, Talence, France[6]; and Département de Gynécologie Obstétrique, Centre Hospitalier Universitaire Michallon, Grenoble, France[7]

Received 14 September 2009/Returned for modification 6 November 2009/Accepted 22 January 2010

Vascular endothelium (VE), the monolayer of endothelial cells that lines the vascular tree, undergoes damage at the basis of some vascular diseases. Its integrity is maintained by VE-cadherin, an adhesive receptor localized at cell-cell junctions. Here, we show that VE-cadherin is also located at the tip and along filopodia in sparse or subconfluent endothelial cells. We observed that VE-cadherin navigates along intrafilopodial actin filaments. We found that the actin motor protein myosin-X is colocalized and moves synchronously with filopodial VE-cadherin. Immunoprecipitation and pulldown assays confirmed that myosin-X is directly associated with the VE-cadherin complex. Furthermore, expression of a dominant-negative mutant of myosin-X revealed that myosin-X is required for VE-cadherin export to cell edges and filopodia. These features indicate that myosin-X establishes a link between the actin cytoskeleton and VE-cadherin, thereby allowing VE-cadherin transportation along intrafilopodial actin cables. In conclusion, we propose that VE-cadherin trafficking along filopodia using myosin-X motor protein is a prerequisite for cell-cell junction formation. This mechanism may have functional consequences for endothelium repair in pathological settings.

The endothelium is composed of a monolayer of endothelial cells that lines the vascular tree. Hemodynamic forces, immune-mediated mechanisms, or drug ingestion can injure the endothelium (35). These types of damage are frequently accompanied by a loss of endothelium integrity, an increase in vascular permeability, and possibly by a detachment of endothelial cells from vascular walls (14). These alterations can be circumvented by initiating rapid repair mechanisms that reestablish endothelium integrity and consequently reduce the extent of vascular diseases. The molecular mechanisms at the basis of the endothelium repair process remain elusive, but it can be assumed that the reconstitution of endothelium integrity requires cell-cell junction rebuilding.

In the endothelium, intercellular adherence is maintained by tight and adherens junctions. Adherens junctions are particularly crucial in controlling the formation and maintenance of interendothelial adhesion and constitute dynamic structures that undergo remodeling in migrating as well as resting cells (31). They are essentially composed of vascular endothelial-cadherin (VE-Cad) (22), an adhesive receptor able to elaborate homophilic/homotypic interactions via its extracellular domain and to recruit, through its cytoplasmic tail, partners such as α-, β-, and γ-catenins and p120 (1). Catenins, in turn, promote the association of the adherens junction with the actin cytoskeleton, another player regulating vascular endothelial barrier function, by molecular mechanisms that are incompletely defined (8). Although there is a general agreement about the critical role played by actin filaments in the maintenance of mature cell-cell junctions (27, 41), their precise role in the elaboration of premature adherens junctions is poorly understood. Some studies indicate that cells form intercellular junctions by a dynamic process driven by actin polymerization (38). It was proposed but, to our knowledge not firmly demonstrated, that cell-cell junction formation is initiated by the production of filopodia emanating from neighboring cells (3, 30, 39, 42). Filopodia lead to the elaboration of puncta, which correspond to microdomains where cadherin molecules concentrate together with their intracellular partners (3). These puncta spatially coincide with cell membrane attachment sites for actin filaments (2). The mechanism by which puncta are elaborated remains to be elucidated.

Filopodia are highly dynamic structures filled with bundles of linear actin filaments (15). Their protrusion is driven by actin polymerization taking place at filament barbed ends that are mainly located at filopodium tips (24). The precise mechanisms of the nucleation and elongation of filopodia are con-

* Corresponding author. Mailing address: iRTSV, APV, INSERM U882, CEA-Grenoble, 17 Rue des Martyrs, 38054 Grenoble Cedex 9, France. Phone: 33 4 38 78 92 72. Fax: 33 4 38 78 49 64. E-mail: danielle.gulino@cea.fr.

‡ S.A. generated Fig. 1, 3, and 4, as well as Fig. 7 to 15 and all movies. C.D. and S.H. generated Fig. 5, A.C.-P. generated Fig. 2, and O.L. and M.D. generated Fig. 6. J.P.S. provided human umbilical cords. P.H. is the head of the laboratory and provided grants, equipment, and discussions, whereas E.H. helped write this article. D.G.-D. conceived experiments, interpreted data, and wrote the article.

† Supplemental material for this article may be found at http://mcb.asm.org/.

▽ Published ahead of print on 1 February 2010.

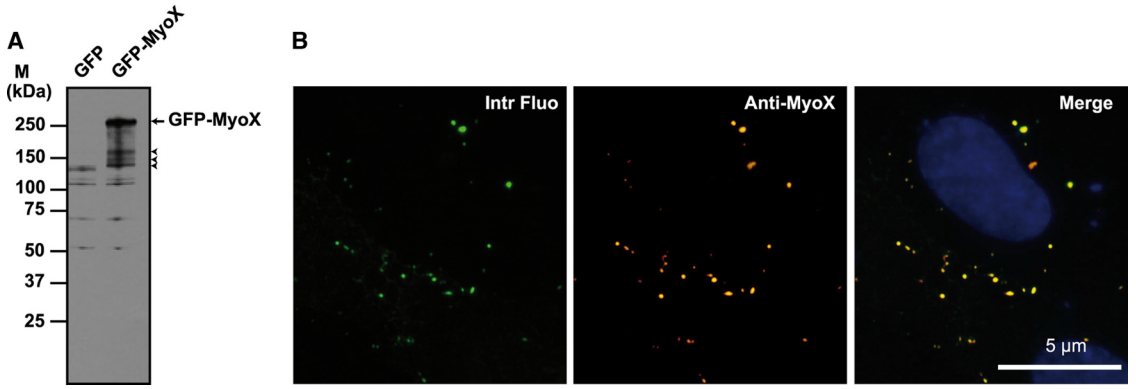

FIG. 1. Biochemical characterization of the anti-MyoX antibody. (A) The rabbit polyclonal anti-myosin-X antibody identified a polypeptide band of the expected molecular mass in lysates of GFP-MyoX-expressing CHO cells. In contrast, no specific band was detected in lysates of GFP-expressing CHO cells, indicating that no MyoX is expressed in CHO cells. The arrow points out intact GFP-MyoX, whereas arrowheads indicate degradation products. M, molecular mass markers. (B) CHO cells expressing GFP-MyoX were immunofluorescently stained for MyoX. We observed that the intrinsic fluorescence of the GFP tag (Intr Fluo) colocalized with the immunostaining of MyoX (Anti-MyoX), thus attesting to the specificity of the antibody for MyoX.

troversial. In fact, two mechanisms for their formation have been proposed, each using different sets of actin-regulating proteins. According to the "convergent elongation model," filopodia are continuously initiated by the elongation of preexisting lamellipodial actin filaments (34). This remodeling of actin filaments should require the branching activity of Arp2/3 (29), the F-actin-bundling activity of fascin along filopodium shafts and the anticapping activity of Ena/VASP at the barbed ends of actin filaments (4). In the opposing model, it was proposed that some members of the formin family such as Dia2 perform all these activities (17). Indeed, *in vitro*, Dia2 nucleates linear actin filaments, accelerates actin polymerization, and protects barbed ends from capping proteins, thus slowing actin depolymerization (7, 17). Additionally, new players such as myosin-X (MyoX), able to induce filopodium formation, have been recently discovered.

Here, using cryo-electron microscopy (cryo-EM), we show that VE-cadherin is not exclusively located at cell-cell junctions but is also present along and at the tip of filopodia in sparse endothelial cells. By video microscopy, we observed that VE-cadherin migrates along filopodia in forward and backward movements. We hypothesized that motor proteins of the myosin family may be involved in the VE-cadherin transportation along filopodia. We considered MyoX as a potential candidate for promoting VE-cadherin trafficking.

Myosins participate in a range of diverse cellular processes such as cell migration, membrane trafficking, and formation of cellular protrusions. They share conserved structural features such as a motor domain located at their N termini that can bind to actin filaments and hydrolyze ATP to produce movement and force. At their C termini, members of the unconventional myosin family such as myosin-VII, -X, -XII, and -XV exhibit a myosin tail homology 4 domain (MyTH4) followed by a FERM (band 4.1 protein, ezrin, radixin, and moesin) domain that confers upon them with the ability to perform unique cellular functions (6). A fascinating feature of MyoX is that it uses its motor activity to move along the intrafilopodial actin filaments. This probably allows MyoX to carry cargoes along filopodia. Potential cargoes are the β-chains of integrins, recently reported to directly interact with the FERM domain of MyoX (43), and Mena/VASP, which is synchronously transported with MyoX toward the tip or the base of filopodia (36). In addition to its motor and transport functions, MyoX also promotes the formation of filopodia (5, 9, 37). Hence, MyoX overexpression stimulates filopodium growth (5), whereas its knockdown decreases filopodium formation (9, 28, 37).

Herein, we discovered that MyoX is colocalized with VE-cadherin in filopodia and moves synchronously with it. Using immunoprecipitation (IP) experiments and pulldown assays, we demonstrated that MyoX interacts with the VE-Cad–catenin complex. Our data thus support a role of MyoX in the transportation of VE-cadherin along intrafilopodial actin. The forward MyoX-mediated transport facilitates the accumulation of VE-Cad at the tips of filopodia, where VE-Cad can interact with partners of adjacent cells, thus establishing preliminary cell-cell contacts. Formation of these early cell-cell contacts can be inhibited by blocking MyoX transport capacity. At filopodium tips, VE-Cad linked to MyoX, but not engaged in homophilic interactions, may also be transported backwards to the cell body by the actin retrograde flow. Once at the lamellipodium edge, VE-Cad can be picked up again by newly formed filopodia. Our data suggest that MyoX-mediated transport of the VE-Cad–catenin complex along filopodia is a key event required for the early steps of formation of cell-cell contacts, a process that may be of functional importance in endothelium repair and angiogenesis.

MATERIALS AND METHODS

Drugs and antibodies. Fibronectin, latrunculin B (LaB), fluorescein isothiocyanate (FITC)- or rhodamine-conjugated phalloidin, and monoclonal antibody (MAb) against α-catenin and β-actin were from Sigma-Aldrich. The MAb antibodies against β- and γ-catenins and p120 were from Transduction Laboratories. The affinity-purified polyclonal antibody (pAb) against human MyoX from SDI (Newark, DE) was used in Western blot, immunoprecipitation, and immunofluorescence analyses. Its biochemical characterization is presented in Fig. 1. The pAb anti-β1 integrin antibody was a generous gift from C. Albigès-Rizo (25), while the anti-glutathione *S*-transferase (anti-GST) pAb was from GE Healthcare. The anti-Cad3 pAb was used to immunoprecipitate the VE-Cad-based complex (18); (19). The anti-VE-Cad pAb C-19 (Santa Cruz Biotechnology) and

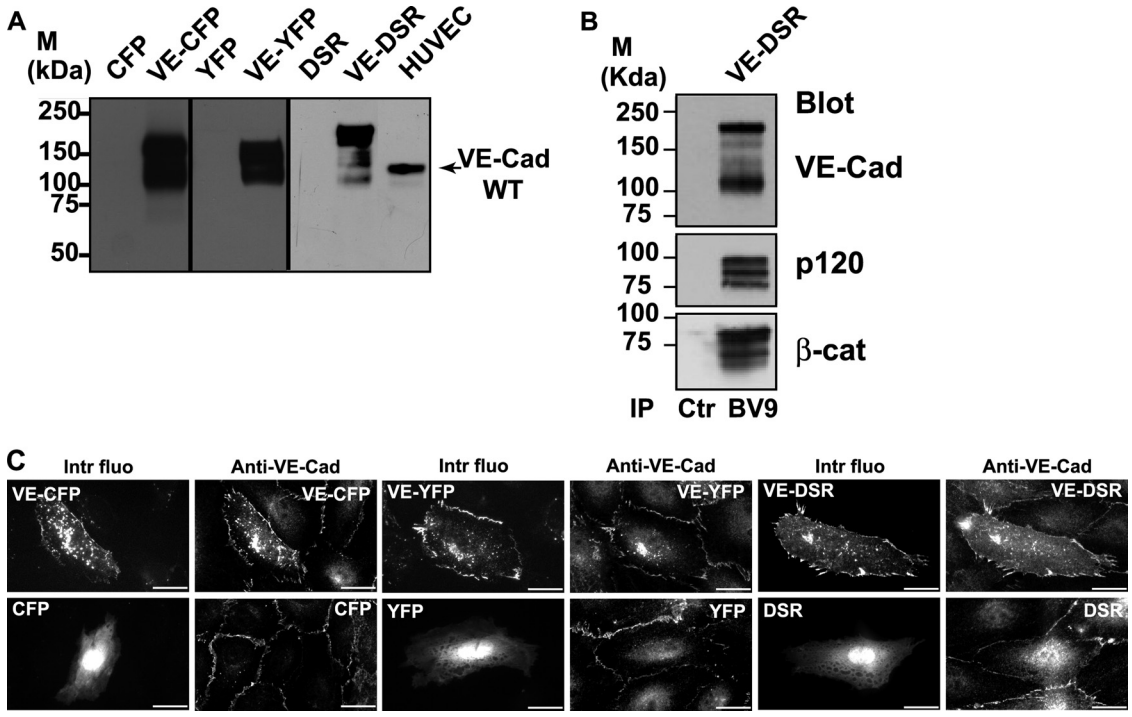

FIG. 2. Characterization of the fluorescent proteins VE-CFP, VE-YFP, and VE-DSR. (A) Biochemical characterization of VE-CFP, VE-YFP, and VE-DSR. cDNA constructs expressing CFP, VE-CFP, YFP, VE-YFP, DSR, and VE-DSR were transfected in CHO cells. At 24 h posttranfection, lysates of these transfected cells were analyzed by Western blotting. The anti-VE-Cad MAb BV9 identified polypeptide bands of 165, 150, and 190 kDa corresponding to the expected sizes for VE-CFP, VE-YFP and VE-DSR, respectively. These bands were not detected in lysates of CHO cells expressing CFP, YFP, and DSR. In HUVECs used as a control, the wild-type (WT) form of VE-Cad was detected as a 135-kDa polypeptide band. (B) Coimmunoprecipitation of VE-DSR with catenins. Anti-VE-Cad immunoprecipitation (IP BV9) was performed on VE-DSR-expressing CHO cells prior to being resolved on a 4 to 12% gradient gel, electrotransferred, and probed successively for VE-Cad, p120, and β-catenin (β-cat). As control, an immunoprecipitation performed on VE-DSR-expressing CHO cells using rabbit nonimmune IgG (Ctr) was analyzed in parallel. Molecular mass markers (M) are given at the margin of the panel. (C) Localization at cell-cell contacts of exogenous VE-CFP, VE-YFP, and VE-DSR transiently expressed in HUVECs. HUVECs expressing VE-CFP, CFP, VE-YFP, YFP, VE-DSR, and DSR were immunofluorescently stained for VE-Cad and observed by confocal microscopy. Then, the intrinsic fluorescence of the CFP, YFP, and DSR tags (Intr fluo) was compared to the immunofluorescent staining (Anti-VE-Cad). As expected, the three fluorescent VE-Cad proteins were mainly expressed at cell-cell junctions and on filopodia recapitulating the staining pattern of endogenous VE-Cad. In contrast, the proteins CFP, YFP, and DSR did not present a specific localization. Bars, 20 μm.

MAb BV9 (11) (Abcam) were used in Western blot experiments. The monoclonal antibody (MAb) BV9 is directed against the extracellular domain and the polyclonal antibody (pAb) C-19 against the 19-amino-acid peptide at the VE-Cad C terminus. The secondary Cy2- or Cy3-conjugated antibodies were from Jackson Immunoresearch Laboratories, the Cy5-conjugated antibodies were from GE Healthcare, and Alexa 488, 555, and 633 were purchased from Invitrogen.

Cell culture. Human umbilical vein endothelial cells (HUVECs) were isolated and cultured as previously described (16). Only cells on passage 2 were used. HeLa cells and CHO cells were respectively cultured in Dulbecco's modified Eagle's medium (DMEM; Invitrogen) or in mimimal essential medium alpha (α-MEM; Invitrogen) supplemented with 10% fetal calf serum (FCS) and antibiotics.

cDNA constructs and protein expression in *E. coli*. A cDNA fragment containing the sequence encoding the FERM domain of bovine MyoX (K1767 to V2051) (6) was produced by PCR using the oligonucleotides 5′-GTGGATCCA AGTTTGAAAAGCTGGCCGCC-3′ (forward) and 5′-TCGACCCGGGTCAC ACGGAGCGCGAGGTGCTGTA-3′ (reverse). After digestion with BamHI and XmaI, the PCR fragment was then inserted into pGEX-4T1 (GE Healthcare) to elaborate the vector pGEX-4T1-FERM coding for the FERM domain of MyoX fused with an N-terminus GST (GST-FERM). The protein GST-FERM was then produced in BL21-RIL (Stratagene) and purified from inclusion bodies dissolved in urea. The protein was *in vitro* refolded by rapid dilution in 50 mM Tris-HCl (pH 8) buffer containing 150 mM NaCl prior to being captured on a glutathione-Sepharose column. The 59-kDa recombinant protein was purified to homogeneity after elution using reduced glutathione. The His-tagged cytoplasmic domain of VE-Cad was obtained as previously described (40).

Eukaryotic expression vectors. The vector encoding green fluorescent protein (GFP)-MyoX was kindly provided R. Cheney (5). Pro-VE-Cad cDNA was subcloned in the Clontech vectors pAmCyan1-N1 and pZsYellow1-N1 to express VE-Cad C-terminally fused with cyan fluorescent protain (VE-CFP) and yellow fluorescent protein (VE-YFP). Additionally, Pro-VE-Cad was also C-terminally fused with the tandem dimer of DsRed, tdimer2, using the vector pcDNA3.1-DsRed previously described (12). This protein, designated VE-DSR, remained monomeric because of its fusion with a tandem dimer of DsRed. Indeed, formation of intramolecular contacts between the tandem DsRed moieties within the same polypeptide prevents protein oligomerization (12). Additionally, the tandem DsRed motif rendered VE-DSR resistant to photobleaching and consequently perfectly well-adapted to video microscopy experiments. The characterization of these fluorescent proteins is presented in Fig. 2. The specificity of VE-DSR and GFP-MyoX localization in double-fluorescently transfected HUVECs was also controlled (Fig. 3).

To express in HUVECs and CHO cells the protein GST-FERM-DSR, the eukaryotic expression vector pcDNA3.1-GST-FERM-DSR was constructed by amplifying by PCR the cDNA coding for the GST-FERM protein. This was performed using the *Escherichia coli* expression vector pGEX-4T1-FERM and the primers 5′-CACATCTAGAATGTCCCCTATACTAGGTTAT-3′ and 5′-G CAGATATCACGGAGCGCGAGGT-3′. Following digestion by XbaI and EcoRV, this PCR fragment was then introduced in the vector pcDNA 3.1-DSRed to generate the eukaryotic expression vector pcDNA-GST-FERM-DSR,

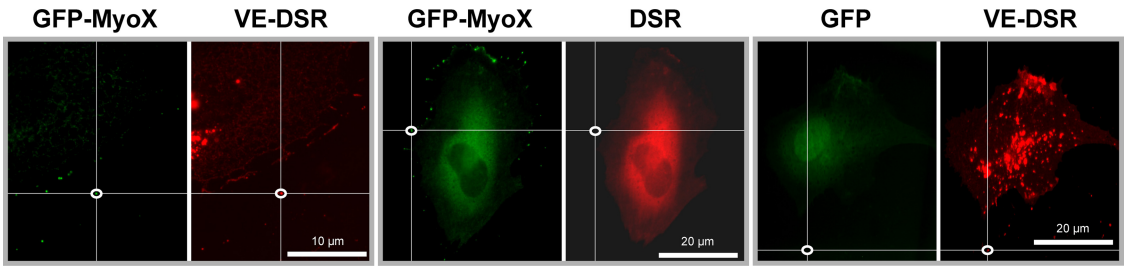

FIG. 3. Specificity of localization of VE-DSR and GFP-MyoX in double-fluorescently transfected HUVECs. To control the specificity of GFP-MyoX localization, HUVECs coexpressing either GFP-MyoX and VE-DSR (panels at left) or GFP-MyoX and DSR (middle panels) were analyzed in green and red fluorescence channels. Using ImageJ, the fluorescent intensities (I) of GFP-MyoX spots (delimited by ellipses) were measured and compared to the fluorescent intensities of the superimposed areas in the other channel. While the mean value for the $I_{\text{GFP-MyoX}}/I_{\text{VE-DSR}}$ ratio ranges around 1 (20 measurements from 5 images), that of the $I_{\text{GFP-MyoX}}/I_{\text{DSR}}$ ratio varied between 3×10^5 and infinite (20 measurements from 5 images). Similarly, to control the specificity of VE-DSR localization, HUVECs coexpressing GFP and VE-DSR were analyzed in parallel for fluorescent localization (panels at right). While the mean value for the $I_{\text{VE-DSR}}/I_{\text{GFP-MyoX}}$ ratio ranges around 1, that of the $I_{\text{VE-DSR}}/I_{\text{GFP}}$ ratio varied between 1×10^5 and infinite (20 measurements from 5 images). From ratio-metric quantification, it can be deduced that the localization of VE-DSR or GFP-MyoX is not disturbed by GFP- and DSR-associated fluorescence, respectively.

coding for GST-FERM-DSR. Similarly, to express in HUVECs and CHO cells, the protein GST-DSR, the eukaryotic expression vector pcDNA-GST-DSR was elaborated by amplifying the cDNA coding for GST. This was made using the vector pGEX-4T1 (GE-Healthcare) and the primers 5′-CCGCTCGAGATGTC CCCTATACTAGGTTATTG-3′ and 5′-GCGGATCCTTATCCGATTTTGGA GGATGGTC-3′. Following digestion by XhoI and BamHI, this fragment was inserted into the eukaryotic expression vector pcDNA-DSRed to generate the vector pcDNA-GST-DSR coding for GST-DSR.

Transfections. Once seeded on glass coverslips or Labtek I (Nunc, Rochester, NY), HUVECs were transiently transfected using 200 nM polyethylenimine (PEI; Sigma-Aldrich) added in cell medium culture devoid of serum during 45 min at 37°C. HeLa and CHO cells were transfected using Exgen 500 (Euromedex) according to the manufacturer's protocol.

Immunoprecipitation and GST pulldown assays. For pulldown assays, cell lysates (57 cm^2) were incubated overnight at 4°C with 200 μl of glutathione beads coupled to either GST or GST-FERM proteins in the presence or absence of 100 μM latrunculin B (LaB). After three washing steps in lysis buffer, consisting of 10 mM PIPES [piperazine-*N*,*N*′-bis(2-ethanesulfonic acid), pH 7.7], containing 100 mM NaCl, 300 mM sucrose, 3 mM $MgCl_2$, 1 mM EDTA, and 0.5% NP-40, pulled-down proteins were eluted with 100 μl washing buffer containing 20 mM reduced glutathione and then boiled with Laemmli buffer containing β-mercaptoethanol.

For immunoprecipitations, endothelial cell or CHO monolayers (57 cm^2) were lysed for 5 min at 4°C and scrapped in 500 μl radioimmunoprecipitation assay (RIPA) buffer (phosphate-buffered saline [PBS], pH 7.4, 150 mM NaCl, 1 mM $MgCl_2$, 0.5% deoxycholate, 1% Triton X-100, 0.1% SDS, 1 mM ATP, containing a protease inhibitor cocktail). Prior to preclearing, cell lysates were treated with latrunculin B as mentioned for pulled-down experiments. Precleared lysates were immunoprecipitated with the polyclonal anti-MyoX (4 μg) or anti-VE-Cad (4 μg) antibodies coupled to 1.6 mg of protein A-Sepharose (Sigma). Immune complexes were washed three times with RIPA buffer prior to being eluted with 2× Laemmli buffer for 10 min at 100°C and reduced with β-mercaptoethanol.

SDS-PAGE and Western blot analysis. MyoX immunoprecipitations were separated by electrophoresis in MOPS (morpholinepropanesulfonic acid) buffer (Bio-Rad) on precast Criterion XT 4 to 12% gradient Bis-Tris gels (Bio-Rad). The gels were transferred 1 h (300 mA) to Immobilon membrane (Millipore) using a Tris-glycine buffer. Then, membranes were blocked with 5% nonfat dry milk, and proteins from total cell extracts, immunoprecipitates, or pulldown assays were detected by specific primary antibodies as specified followed by horseradish peroxidase-conjugated goat anti-mouse or goat anti-rabbit immunoglobulin reagents (Sigma). The immunoreactive bands were revealed using the ECL enhanced chemiluminescence Western blot detection kit (Amersham).

Immunofluorescence labeling of fixed HUVECs. For all immunostainings except MyoX, cells were fixed for 20 min with 3% paraformaldehyde (PFA) and permeabilized using 0.5% Triton X-100 for 3 min. The protocol to visualize MyoX is adapted from reference 23. Briefly, after two rinsing steps in calcium- and magnesium-containing PBS, cells kept for 3 min on ice were prepermeabilized for 3 min in MyoX-F buffer (10 mM PIPES, pH 6.8, 50 mM NaCl, 3 mM $MgCl_2$, 300 mM sucrose) with 0.5% Triton X-100 containing an inhibitor cocktail (Roche) prior to being fixed for 20 min at room temperature with chilled MyoX-F buffer containing 4% PFA. After a blocking step in 5% fetal calf serum-containing PBS during 1 h, cells were incubated with primary antibodies overnight at 4°C and subsequently incubated with appropriate secondary antibodies.

Microscopy. For video microscopy experiments, once seeded on Lab-Tek I chambers, HUVECs and HeLa cells were maintained in phenol red-deprived M199 (supplemented with low serum growth supplement, 20% fetal calf serum, and antibiotics) and phenol red-deprived DMEM (supplemented with 10% fetal calf serum and antibiotics) cell culture media, respectively. Confocal video microscopy images were collected on a Zeiss LSM510 confocal microscope equipped with a heating workplate, a humidifier, a CO_2 delivery system, and using either a ×63 Plan Apochromat objective (oil, 1.45 numerical aperture [NA], pH 3) or a ×40 Plan-Neofluar objective (oil, 1.30 NA, pH 3) (photonic microscopy-cellular imaging platform of Institut Albert Bonniot, Grenoble, France). The time between images was typically 1 to 3 min. Phase-contrast images were always coacquired with YFP in order to reduce the delay between frames. Epifluorescence video microscopy images were collected sequentially on an IX71 (Olympus) microscope equipped with a heating workplate, a humidifier, and a CO_2 delivery system and using a ×40 Plan Apochromat (oil, 1.0 NA, pH 3) or a ×40UApochromat (oil, 1.35 NA) objective and an ORCA-ER camera (Hamamatsu). Typical time between frames for epifluorescence videomicroscopy varies from 100 ms to 3 min. In general, cells were imaged over periods of 1 to 180 min. Confocal images on fixed cells were collected sequentially using a Leica TCS-SP2 confocal microscope (Leica Manheim, Germany) equipped with a ×63 HCX Plan Apochromat objective (oil, 1.4 NA). Epifluorescence images on fixed cells were acquired using an Axioplan 2 microscope (Zeiss) equipped with a ×100 AchroPlan (oil, 1.25 NA) or ×50 AchroPlan (oil, 0.9 NA) and an AxioCam MR camera. Fluorescence filters were chosen and tested on each combination of plasmid constructions to abolish fluorescence overlap. Only microscope proprietary software was used to acquire images.

Image processing. Each time-lapse confocal image corresponds to the projection of four 500-nm optical sections. Movies were treated and edited using ImageJ and Adobe After Effects 6.5 and exported using Quick Time Pro 7.4 with H.264 codec. For fixed cells, images were treated and mounted using Adobe Photoshop CS 2 and Illustrator CS 2.

Patch velocity measurements and statistics. Kymographs were generated using ImageJ and Multiple kymograph plugin. In fact, kymographs were generated by analyzing several filopodia from different HeLa cells. Two typical kymographs illustrating the forward (A) and backward (B) movements of GFP-MyoX are shown in Fig. 4. The two-sample t test was used to determine if the average rates for forward movements of VE-DSR and GFP-MyoX, derived from velocity histograms, were equivalent.

Cryo-electron microscopy. HUVECs were plated on holey carbon fibronectin-precoated nickel grids. After a 24-h postseeding period, cells were fixed with paraformaldehyde at room temperature. VE-Cad was then stained with the monoclonal antibody BV9 and protein A conjugated to 10-nm colloidal gold particles. Cells were submitted to a postfixation step using glutaraldehyde. For cryo-EM observation of VE-Cad, grids were rapidly plunged into a liquid ethane bath cooled with liquid nitrogen (Leica EM CPC, Vienna, Austria) and maintained at a temperature of approximately −170°C using a cryo-holder (Gatan,

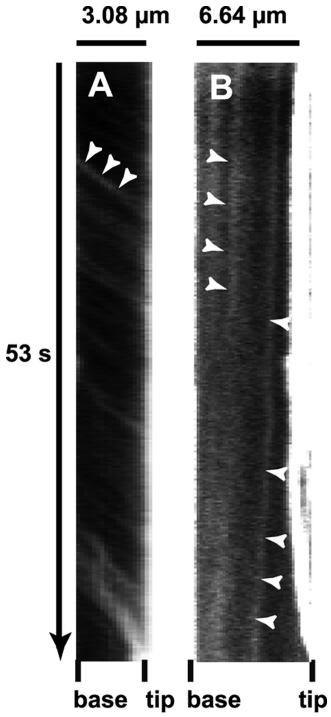

FIG. 4. Kymographs illustrating the forward and backward movements of GFP-MyoX. (A) Kymograph of a selected filopodium emanating from GFP-MyoX-expressing HeLa cells imaged at 25°C using a ×40 lens (NA 1.35), a pixel size of 162 nm, and a frame rate of 5.6 images s^{-1} over 300 frames. Numerous faint tracks sloped down toward the filopodium tip, illustrating the forward movement of GFP-MyoX. Note that patches of GFP-MyoX move at a relatively similar constant velocity. (B) Kymograph of a selected filopodium emanating from a GFP-MyoX-expressing HeLa cell imaged as in Fig. 4A. Two faint tracks sloped down toward the filopodium base, illustrating the backward movement of MyoX.

Pleasanton, CA) prior to being observed using an FEI Tecnai F20 electron microscope (Eindhoven, Netherlands) operating at 200 kV under low-dose conditions. Images were recorded with a 2,000-by-2,000 low-scan charge-coupled device (CCD) camera (Gatan).

RESULTS

Filopodia establish the preliminary endothelial cell-cell contacts. To elucidate the role of filopodia in the formation of early endothelial cell-cell contacts, HUVEC monolayers were costained for VE-cadherin and actin. As expected, costaining revealed that the most mature junctions exhibited a continuous thin VE-Cad labeling close to circumferential actin cables (Fig. 5, middle and upper panels). However, in preliminary cell-cell contacts, VE-Cad labeling exhibited a characteristic zigzag staining dotted with residual randomly distributed intercellular gaps (Fig. 5, middle and lower panels). These newly formed intercellular contacts were composed of multiple protrusions where VE-Cad colocalized with radially oriented actin fibers (Fig. 5, lower panels). Cryo-electron microscopy confirmed and showed more precisely that, in subconfluent HUVECs, VE-Cad molecules are distributed along and at the tips of protrusions. The electron micrographs also revealed the presence of actin filaments aligned in tight parallel bundles within

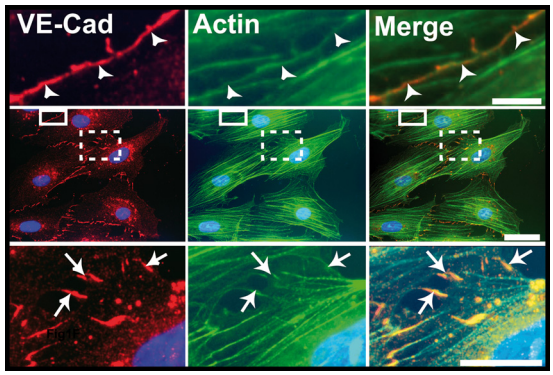

FIG. 5. Localization of VE-Cad in subconfluent HUVECs. Images in the central row show a HUVEC monolayer immunolabeled for VE-Cad (red, left) and actin (green, center), as well as the merge (right). The selected enlargements of a mature cell-cell junction (continuous frame) and an immature junction (dotted frame) are shown in the upper and lower rows, respectively. In mature junctions, VE-Cad and cortical actin fibers are located at the cell circumference (arrowheads, upper row). In contrast, in immature junctions, VE-Cad colocalizes with radial actin fibers along filopodial extensions bridging adjacent cells (arrows, lower row). Bars: 2 μm, upper; 10 μm, middle; and 5 μm, lower.

these protrusions that, consequently, could be functionally defined as filopodia (Fig. 6) (34).

VE-Cad molecules navigate on filopodia. We then used video microscopy to examine whether VE-Cad is able to move along filopodia. To visualize VE-Cad, various constructs coding for VE-Cad C-terminally fused to fluorescent DsRed (red), YFP (yellow), and CFP (cyan) were elaborated to express VE-DSR, VE-YFP, or VE-CFP, respectively (Fig. 2). It must be noted that these cDNA constructs were designed to produce fluorescent VE-Cad molecules that remained monomeric and interact with catenins (reported in Materials and Methods; Fig. 2).

At subconfluency, HUVECs emitted numerous filopodia that formed bridges between neighboring cells (Fig. 5). In preliminary confocal video microscopy experiments performed on VE-YFP-expressing HUVECs, at a frame rate of 1 image min^{-1}, we observed that some patches of VE-YFP adopted linear trajectories by moving along preestablished filopodia (Fig. 7; see Movie S1 in the supplemental material). In contrast, no such movement was seen for YFP (Fig. 7; see Movie S2 in the supplemental material). In a second type of experiments, sparse living HUVECs transiently expressing VE-DSR were observed by video microscopy using a frame rate of 3 images s^{-1} (see Movie S3 in the supplemental material). Under these conditions, isolated cells emitted numerous free filopodia along which faint VE-DSR particles moved rapidly. VE-DSR trajectories appeared nearly linear and were more rapid in Movie S3 than those observed by slow-frame-rate confocal video microscopy in Movie S1. In contrast, such a rapid traffic was not observed in HUVECs overexpressing control DSRed (see Movie S4 in the supplemental material), thereby indicating that trafficking is due to the VE-Cad moiety linked to the transportation machinery. Altogether, the data suggest that VE-Cad molecules navigate on filopodia, probably through an actin-dependent mechanism excluding the possibility that membrane diffusion is at the basis of VE-Cad motion.

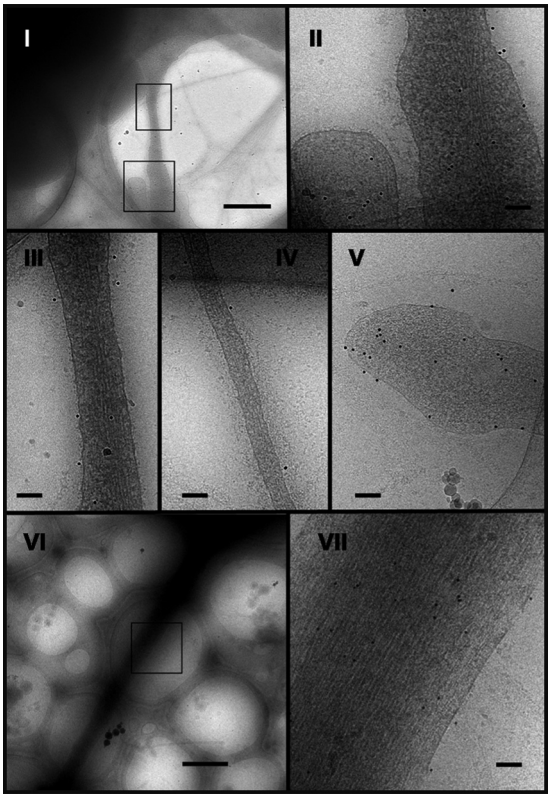

FIG. 6. Localization of VE-Cad at the surface of HUVEC filopodia by electron microscopy. Living HUVECs were seeded on electron microscopy holey grids and grown for 24 h. After fixation without permeabilization, cells were successively marked with MAb BV9 antibody and protein A-conjugated gold particles to reveal the presence of VE-Cad at the cell surface. They were then vitrified for observation. Electron micrographs revealed filopodia of various diameters and lengths connecting adjacent cells (micrographs I and VI, bars, 1 μm). Higher-magnification images show gold particles dispersed along the length (micrographs II, III, IV, and VII, bars, 100 nm) and at the tip of filopodia (micrograph V, bar, 100 nm). This indicates that VE-Cad is distributed over the surface of filopodia. Furthermore, on large as well as thin filopodia, underneath the plasma membrane, the network of actin fibers could be observed parallel to the filopodium axis (micrograph VII).

Moreover, as shown thereafter, the fast and slow velocities observed for VE-Cad particles corresponded to forward (toward the filopodium tip) and backward (toward the filopodium basis) motions, respectively.

The motor protein myosin-X interacts with the VE-Cad–catenin complex. As VE-Cad is able to move along filopodia, we hypothesized that VE-Cad is directly or indirectly linked to intrafilopodial actin fibers through an actin motor protein. Myosins constitute a family of actin-dependent motor proteins that support protein carrier function. Endothelial cells expressed several myosin family members such as myosin-II, -VII, and -X. The unconventional myosin-X (MyoX) is a potential candidate for VE-Cad transport since it is located at the filopodium tips of various nonendothelial cell lines (5).

Analysis of HUVEC lysates by Western blotting using anti-MyoX antibody revealed the presence of a 240-kDa band corresponding to full-length MyoX (Fig. 1 and 8A). Additional bands with molecular masses ranging from 100 to 130 kDa were also detected because of MyoX susceptibility to proteolysis (6). Immunofluorescence labeling of subconfluent HUVECs effectively showed punctate staining of MyoX that partially colocalized with VE-Cad (Fig. 8B). After a careful scrutiny of immunofluorescence images, MyoX appeared associated with extrajunctional VE-Cad molecules and not with junctional VE-Cad molecules (Fig. 8B). We speculated that MyoX interacts, at least temporarily, with VE-Cad, thus allowing its cellular transport along intrafilopodial actin fibers. To verify this hypothesis, different approaches such as immunoprecipitation and pull-down assays were used. Hence, analyses of VE-Cad immunoprecipitates by Western blotting using an anti-MyoX antibody revealed the presence of the 240-kDa form of MyoX (Fig. 9 A). Conversely, anti-MyoX immunoprecipitation showed association of MyoX with the uncleaved form of VE-Cad (Fig. 9B). To confirm immunoprecipitation data, GST pulldown assays were performed on HUVEC extracts using the FERM (band 4.1 protein, ezrin, radixin, and moesin) domain of MyoX previously described to be involved in cargo binding (28, 43) and N-terminally coupled to GST (GST-FERM). The GST-FERM fusion protein was first assayed for its capacity to bind integrin β-chains, as previously reported for MyoX (41). Pulldown assays, performed on HUVEC extracts, revealed that GST-FERM retained the capability to interact with the integrin β1 chain, whereas GST did not (Fig. 9F). Importantly, GST-FERM specifically interacted with the uncleaved 135-kDa form of VE-Cad and not with the intracellular truncated 100-kDa form present in HUVEC lysates (Fig. 9C). Moreover, GST-FERM was able to pull down the VE-Cad cytoplasmic partners α- or β-catenins or p120 from HUVEC lysates (Fig. 9D). In contrast, it did not interact with a recombinant fragment that overlapped the amino stretch from A630 to Y784 corresponding to the cytoplasmic region of VE-Cad truncated at its N terminus (40; data not shown). This indicates that MyoX associates with one element of the VE-Cad–catenin complex without disturbing its integrity. In addition, actin, probably incorporated in filaments, was also coprecipitated with GST-FERM and not with GST (Fig. 9E). To exclude the possibility that actin filaments link the VE-Cad–catenin complex to MyoX, filaments were depolymerized in cell extracts with the actin monomer-sequestering drug latrunculin B (LaB) (13). Under these conditions, no actin was precipitated in GST-FERM pulldown assays (Fig. 9E). However, VE-Cad was still pulled down with GST-FERM, indicating that actin cables were not involved in the link between the VE-Cad–catenin complex and MyoX. Finally, substitution in pulldown assays of the FERM domain of MyoX by the FERM domain of moesin did not precipitate VE-Cad, attesting that the results obtained with the FERM domain of MyoX are specific (data not shown). Altogether, our results establish that the FERM domain of MyoX interacts with the VE-Cad–catenin complex.

MyoX transports VE-Cad along filopodia. To examine the temporal and spatial colocalization of VE-Cad and MyoX, VE-DSR and MyoX N-terminally fused with GFP (GFP-MyoX [6]) were coexpressed in HUVECs. We first controlled the specificity of the localization of VE-DSR and GFP-MyoX prior to imaging (Fig. 3). Using video microscopy, we noticed that some patches of GFP-MyoX remained immobile at filopodium tips, while others started from the tips of filopodia dragging VE-DSR clusters backwards (Fig. 10; see Movie S5 in

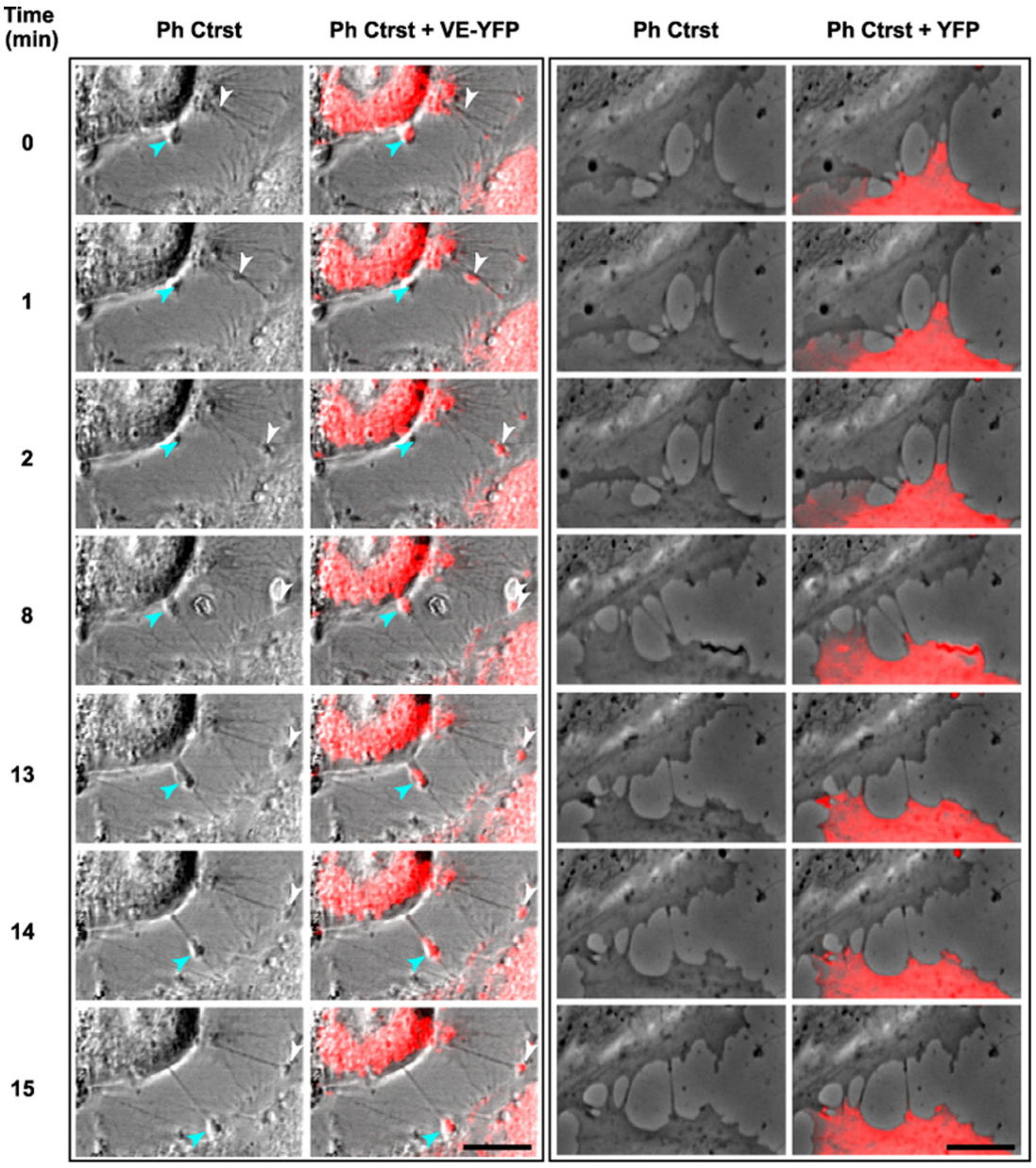

FIG. 7. Selected sequences showing VE-YFP moving along filopodia. Subconfluent HUVECs were transiently transfected with the plasmids expressing either VE-YFP or YFP. At 17 h posttransfection time, confocal video microscopy images were taken every min for 1 h both in phase-contrast (Ph Ctrst) to see the filopodia and in the yellow fluorescence channel. Panels corresponding to VE-YFP-expressing HUVECs (left) showed two distinct patches, indicated by arrowheads, moving sequentially along two filopodia (see Movie S1 in the supplemental material). In contrast, no YFP was detected along filopodia, as illustrated in panels corresponding to YFP-expressing HUVECs (right) (see Movie S2 in the supplemental material). Bars, 10 μm.

the supplemental material). This backward movement was relatively slow and could be observed by video microscopy using a frame rate of 1 image/3 s. In addition, movements of VE-DSR and MyoX patches toward the tips of filopodia (forward motion) were also observed. However, the high displacement rate at 37°C in HUVECs rendered the observation of these movements difficult. To palliate this inconvenience, we chose to image VE-DSR and GFP-MyoX motilities in HeLa cells. These experiments were performed at 25°C to reduce the movement rate (21) since HeLa cells, in contrast to HUVECs, tolerate this temperature. Under these selected conditions, HeLa exhibited 10- to 20-μm-long filopodia, and it was possible to individually track VE-DSR and GFP-MyoX patches over times ranging from 50 to 100 s (see Movies S6 and S7 in the supplemental material). Hence, Movie S7 shows a single patch of GFP-MyoX that colocalized with a single VE-DSR patch and moved synchronously with it on a given filopodium. Both patches moved backwards prior to moving toward the distal tip of the filopodium (full arrowheads). It could be noticed that the backward movement was frequently interrupted

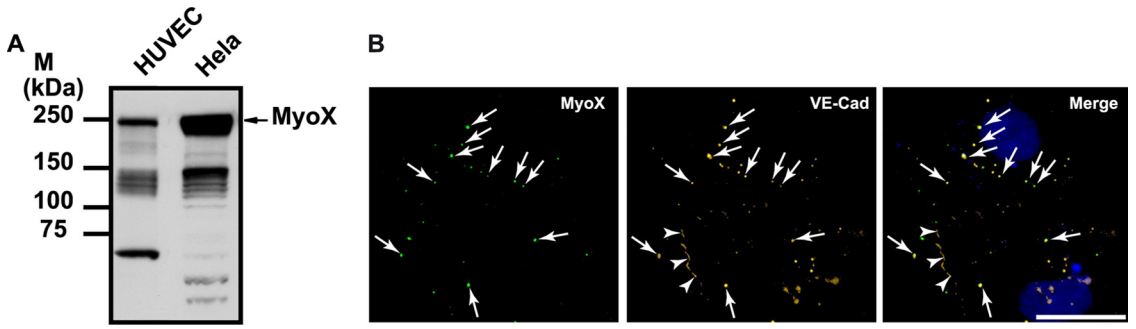

FIG. 8. Expression of MyoX in HUVECs and HeLa cells. (A) Detection of endogeneous MyoX by Western blotting. HUVEC and HeLa cell lysates were analyzed by Western blotting using the anti-MyoX pAb antibody. In HUVECs as well in HeLa cells, the antibody detected a 240-kDa band corresponding to the expected size of MyoX and several bands of lower molecular mass corresponding to MyoX degradation (6). Larger amounts of MyoX were detected in HeLa cells compared to HUVECs. (B) Partial colocalization of endogenous MyoX and VE-Cad along filopodia in subconfluent HUVECs. Subconfluent HUVECs were double labeled for MyoX (left) and VE-Cad (center) with anti-MyoX pAb, anti-VE-Cad MAb BV9, and Alexa 555-labeled goat anti-rabbit and Alexa 488-labeled goat anti-mouse antibodies and Hoechst stain. The merged image is at the right. Arrows point out VE-Cad patches colocalized with MyoX, while arrowheads indicate cell-cell junctions where VE-Cad and MyoX did not colocalize. Bar, 20 μm.

by episodes of pausing (see Movie S7 in the supplemental material). Movie S7 also highlights the difference existing between forward and backward velocities. Altogether, our results on MyoX and VE-Cad colocalization and comigration along filopodia strongly suggest that VE-Cad is transported by a MyoX-dependent mechanism.

Frequently, VE-DSR/GFP-MyoX patches moving forward and backward were individually observed on the same filopodium. To obtain a global vision of protein movements along a given filopodium, the location of each patch was plotted versus time to generate a kymograph. In this kind of projection, each patch movement appears as an individual line directed toward the tip of filopodium for forward movement and toward the filopodium base for backward movement (Fig. 4). The velocity of a large number of individual patches visualized by single-channel video microscopy could be derived from the slope of the tracks in kymographs and reported in histograms showing the velocity profile for each fusion protein (Fig. 11). Hence, we calculated that VE-DSR moved at an average forward rate of 694 ± 174 nm s^{-1} (115 measurements on 35 filopodia) (Fig. 11A) and at an average backward rate of 27 ± 10 nm s^{-1} (38 measurements on 22 filopodia) (Fig. 11C). Similarly, GFP-MyoX kymographs showed that GFP-MyoX moved forward at an average velocity of 649 ± 218 nm s^{-1} (129 measurements on 15 filopodia) (Fig. 11B) and backwards at 25 ± 10 nm s^{-1} (41 measurements on 22 filopodia) (Fig. 11D), as previously described (21). Statistically, according to the two-sample t test, the mean rates for the forward movements of VE-DSR and GFP-MyoX are equivalent ($P > 0.05$).

Double-channel video microscopy experiments were also performed on HeLa cells coexpressing GFP-MyoX and VE-DSR to visualize the synchronous movements of the two fluorescent proteins. Hence, in Fig. 12A and B, dual kymographs showed two selected GFP-MyoX and VE-DSR particles that exhibited synchronous backward (pointed out by arrowheads) and forward (pointed out by arrows) motions. These experiments confirm the cotransport of GFP-MyoX and VE-DSR along filopodia in both directions. Because of the known functions of MyoX as a cargo for protein transport and as an actin motor protein, it is likely that MyoX mediates the transportation of the VE-Cad complex along intrafilopodial actin cables.

MyoX FERM domain overexpression blocks the transportation of VE-CFP. We next tried to test the functional role of MyoX-mediated transport of VE-Cad. We opted for a dominant-negative approach by constructing the fusion GST-FERM-DSR protein consisting of the GST moiety, the FERM domain of MyoX, and DSR (Fig. 13 A). This fluorescent protein was designed to retain the cargo function but to remove the motor function of MyoX. The fusion protein GST-DSR, composed of the GST and the DSR entities, was also elaborated and used as a control (Fig. 13A). The cDNA constructs coding for GST-FERM-DSR and GST-FERM were transiently transfected in CHO cells, and the expression of recombinant proteins was analyzed by Western blotting using the polyclonal anti-GST antibody. As expected, a 110-kDa band and an 80-kDa band were detected in the GST-FERM-DSR and GST-DSR transfectants, respectively (Fig. 13B). Moreover, GST-FERM-DSR interacted with VE-Cad, as attested by immunoprecipitation experiments performed on CHO cells coexpressing VE-Cad and GST-FERM-DSR. In contrast, GST-DSR did not (Fig. 13C).

To prove that VE-Cad sequestration by GST-FERM-DSR is specific, we cotransfected VE-Cad-expressing CHO cells with plasmids coding for GFP-MyoX and either GST-DSR or GST-FERM-DSR. Anti-MyoX immunoprecipitations on cell lysates revealed that the amount of VE-cadherin coprecipitated with MyoX remained nearly unchanged in the presence or absence of GST-DSR (Fig. 13D). In contrast, a slight and reproductive decrease in the amount of VE-Cad immunoprecipitated with MyoX was observed in the presence of GST-FERM-DSR, suggesting that GST-FERM-DSR competes with MyoX for interaction with VE-Cad.

Then, the cellular effect due to VE-Cad sequestration by the FERM domain of MyoX was analyzed in HUVECs coexpressing VE-CFP and GST-FERM-DSR. In double-transfected cells, VE-CFP remained static, concentrated at the periphery of the nucleus, whereas in the absence of GST-FERM-DSR, VE-CFP appeared highly mobile, disseminated

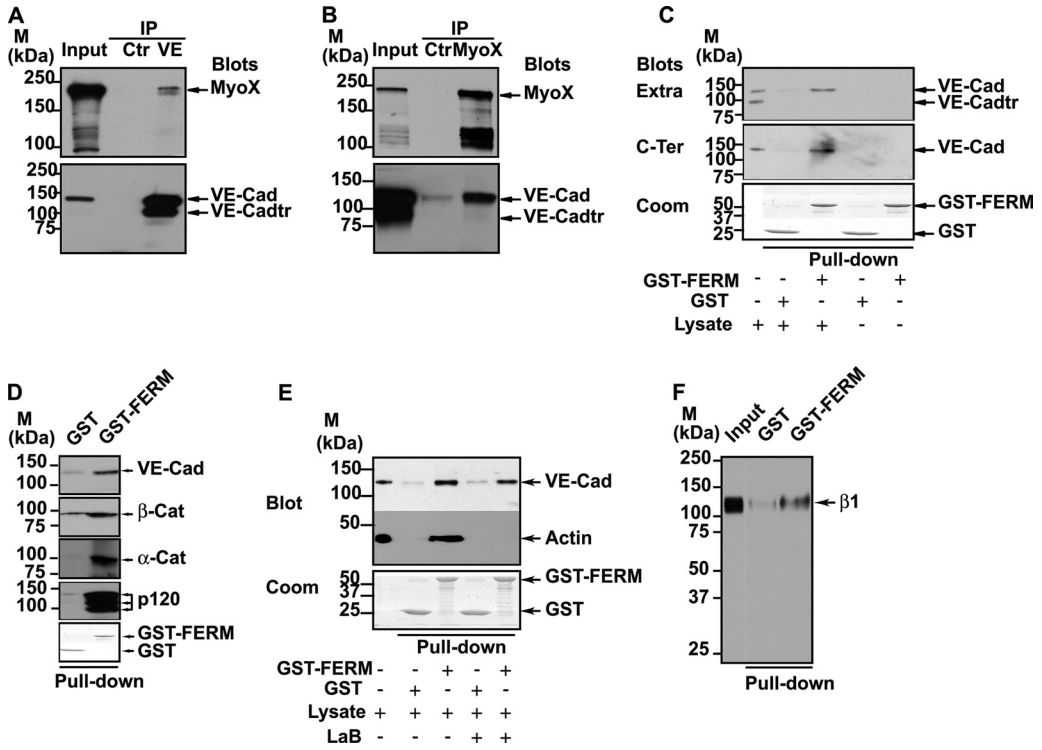

FIG. 9. Association of MyoX to the VE-Cad-based complex. (A and B) Coimmunoprecipitations of endogenous MyoX with endogenous VE-Cad in HUVECs. Anti-VE-Cad (IP VE; A) and anti-MyoX (IP MyoX; B) immunoprecipitations were resolved on 4 to 12% gradient gels, electrotransferred and probed successively for VE-Cad and MyoX. As controls, an aliquot of whole-cell lysate (input) and immunoprecipitations performed on HUVEC lysates using rabbit nonimmune IgG (Ctr) were analyzed in parallel. Note that anti-VE-Cad IP (A) and input analysis by Western blotting (B) revealed the presence of a 100-kDa truncated form of VE-Cad (VE-Cadtr). Molecular mass markers (M) are given at the margins of each panel. (C) Interaction of MyoX with the VE-Cad complex through its FERM domain. GST or GST-FERM immobilized on glutathione beads was incubated with either HUVEC lysates or with buffer. Pulldown assays were revealed with the anti-VE-Cad antibodies directed against the extracellular domain (Extra; MAb BV9) or the cytoplasmic domain (C-Ter, pAb C-19). (Lower panel) Coomassie (Coom) staining of GST proteins used in each pulldown assay. For comparison, aliquots of whole-cell lysates and pulldown assay controls performed without lysate were analyzed in parallel. Note that the antibody C-19 raised against the 19-amino-acid C-terminal peptide of VE-Cad did not recognize VE-Cadtr, indicating that the truncated form of VE-Cad is cleaved at its C terminus. Only the uncleaved form of VE-Cad is coprecipitated with the FERM domain of MyoX. (D) Coprecipitation of catenins with VE-Cad by the FERM domain of MyoX. GST and GST-FERM pulldown assays performed on HUVEC lysates were probed with VE-Cad, α-catenin (α-cat), β-catenin (β-cat), and p120 antibodies. All of these proteins were detected in pulldown assays performed with GST-FERM but not with GST alone. (E) The interaction between the VE-Cad complex and MyoX does not require actin fibers. GST and GST-FERM pulldown assays performed on HUVEC lysates treated (+) or not (−) with latrunculin B (LaB) were sequentially immunoblotted for VE-Cad with C-19 pAb and for β-actin with anti-β-actin MAb. For comparison, an aliquot of whole-cell lysate was analyzed in parallel. (Lower panel) Coomassie staining of GST proteins. In pulldown assays, VE-Cad was precipitated with the domain FERM of MyoX, even in the absence of actin. (F) The recombinant GST-FERM protein interacts with the β1 chain of integrins. GST and GST-FERM pulldown assays performed on HUVEC lysates were immunoblotted for the β1 chain of integrins with the pAb anti-β1 integrin antibody. For comparison, an aliquot of whole-cell lysate (input) was analyzed in parallel. In pulldown assays, the β1 chain of integrins was precipitated with the domain FERM of MyoX.

over the cell surface and at cell-cell junctions (Fig. 14A; see Movie S8 in the supplemental material). We also demonstrated that GST-FERM-DSR concentrates endogenous VE-Cad in the perinuclear area, while GST-DSR did not (data not shown). It can be deduced that, by competing with endogenous MyoX, GST-FERM-DSR could block the transportation of endogenous and exogenous VE-Cad along actin fibers. The absence of transport resulted in an almost total VE-Cad depletion at cell edges (Fig. 14A). Furthermore, cell-cell contacts between GST-FERM-DSR-expressing cells did not stabilize, in spite of the membrane apposition between neighboring cells (Fig. 14B; see Movie S9 in the supplemental material). Numerous intercellular gaps appeared and spaces between opposed cells increased with time. Hence, blockage of MyoX-mediated VE-Cad traffic prevents the adhesion between cell fronts and formation of early cell-cell contacts required for the elaboration of interendothelial junctions.

MyoX/VE-Cad cotraveling operates during wound healing. To obtain additional information about the cellular role of MyoX/VE-Cad cotrafficking, we performed *in vitro* wound-healing assays on GFP-MyoX- and VE-Cad-DSR- overexpressing HUVEC monolayers and followed the early steps of cell-cell junction reconstruction by phase-contrast and fluorescence video microscopy (see Movie S10 in the supplemental material). Movie S10 focused on two noninteracting cells, both coexpressing VE-DSR and GFP-MyoX. These cells emitted very dynamic filopodia. Clearly, several of them operated cooperatively in a confined area to constitute the first cell-cell contacts. At this specific point, it could be observed that VE-Cad accumulated at the filopodium tips, elaborating homophilic interactions as

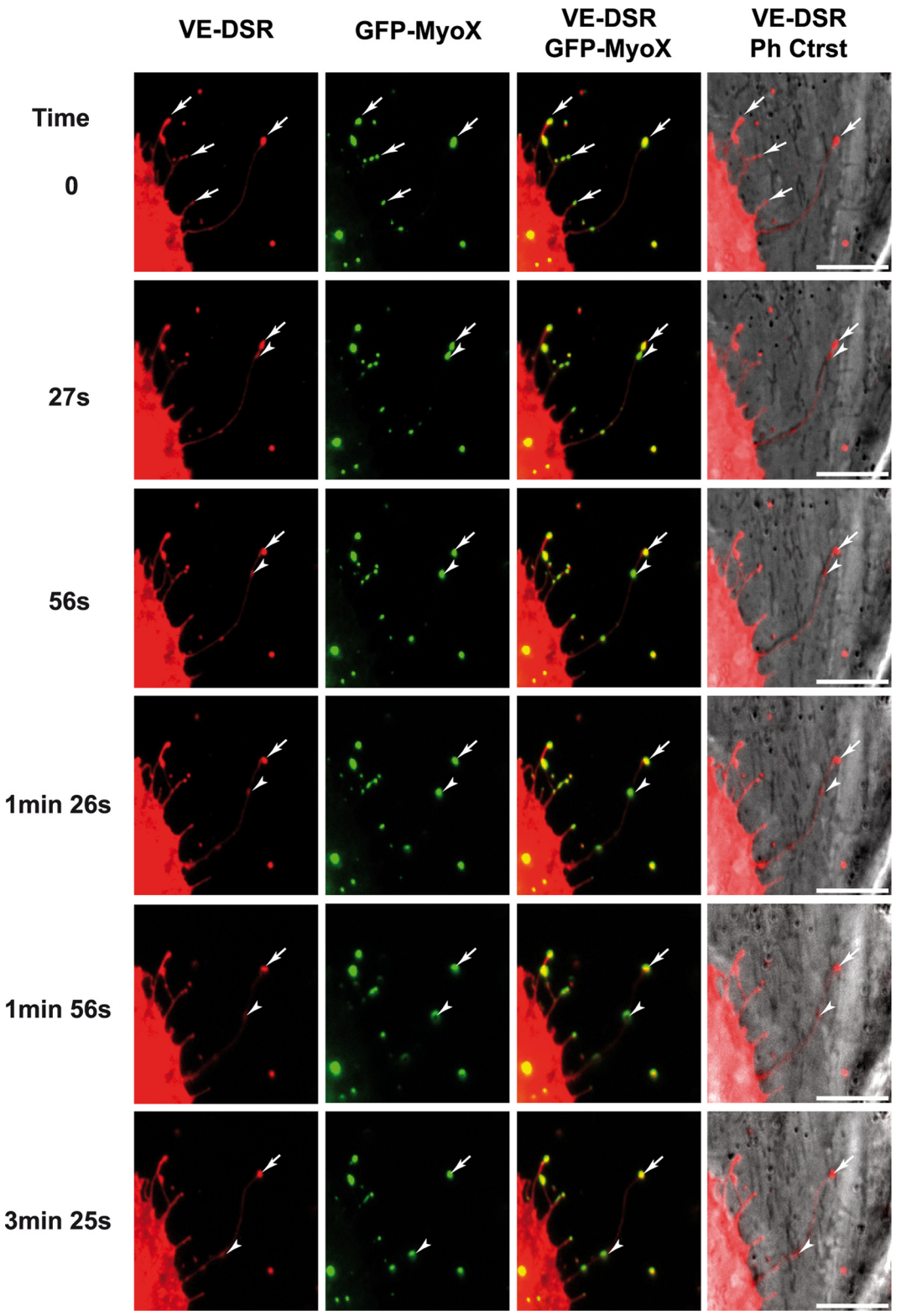

FIG. 10. Selected sequence focusing on the coordinated backward movements of MyoX and VE-Cad. Subconfluent HUVECs, transiently cotransfected with plasmids expressing GFP-MyoX and VE-DSR, were observed by video microscopy at 17 h posttransfection at a frame rate of 1 image/3 s. Full arrowheads and arrows indicate moving and immobile patches, respectively, for VE-Cad and MyoX. Bars, 10 μm.

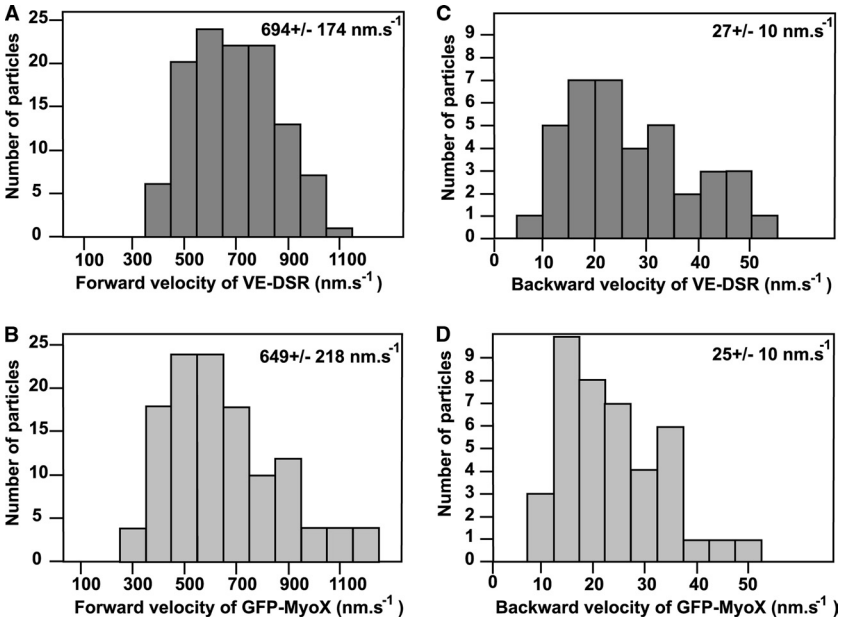

FIG. 11. Velocity histograms for forward and backward movements of VE-DSR and GFP-MyoX patches. Histograms corresponding to the forward movements of VE-DSR (A) and GFP-MyoX (B) patches were generated from 115 and 129 measurements, respectively, while those corresponding to the backward movements of VE-DSR (C) and GFP-MyoX (D) patches were generated from 38 and 41 measurements, respectively. At the top right, the means ± standard deviations are indicated. HeLa cells were imaged at 25°C using a ×40 lens (NA, 1.35), a pixel size of 162 nm, and a frame rate ranging from 3 to 5 images s^{-1}.

soon as filopodia touched the neighboring cell. These very unstable preliminary cell-cell contacts initiated the formation of filopodium-based bridges between the adjacent cells. VE-cadherin-based contacts progressively distributed along the cell edges. The multiplicity of the contact points contributed to cell-cell tightening and to the reduction of the intercellular spaces, leading to a stabilization of the cell-cell junction. In conclusion, these data underlined the role played by MyoX-mediated accumulation of VE-Cad at the tips of filopodia in the elaboration of preliminary endothelial cell-cell contacts, which further progress into wound closure.

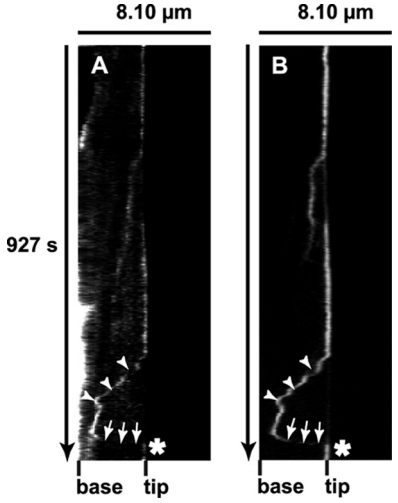

FIG. 12. MyoX and VE-Cad dynamics in living HeLa cells. Shown are synchronous kymographs of a selected filopodium emanating from HeLa cells coexpressing VE-DSR (A) and GFP-MyoX (B) imaged at 25°C using a ×40 lens (NA, 1.35), a pixel size of 162 nm, and a frame rate of 3 images/10 s. The VE-DSR kymograph showed a patch that (i) remained stationary (vertical track), (ii) globally moved backward toward the filopodium base (arrowheads), (iii) abruptly changed direction, and (iv) moved forward (arrows) prior to reaching the filopodium tip. Note that the backward phase was frequently interrupted by pausing events, thus creating a stair-shaped track (arrowheads). This track was perfectly detected in the corresponding GFP-MyoX kymograph illustrating the synchronous movement of VE-DSR and GFP-MyoX patches on a given filopodium.

DISCUSSION

In the present article, we show how the actin cytoskeleton supports VE-Cad transport along filopodia to eventually elaborate primary cell-cell contacts. Indeed, we observed the to-and-fro movements of VE-Cad patches along filopodia and established that this traffic is governed by the motor protein MyoX. A model recapitulating VE-Cad movement modes is proposed in Fig. 15.

Herein, we observed by immunofluorescent staining (Fig. 5) and cryo-electron microscopy (Fig. 6) that VE-Cad is located along filopodia emanating from sparse endothelial cells or forming bridges between neighboring cells. This contrasts with the usual localization of VE-Cad at cell-cell junctions in confluent endothelial monolayers. By video microscopy, we uncovered that VE-Cad navigates along these filopodia (see Movies S1, S3, S5, and S6 in the supplemental material) and suspected that a motor protein of the myosin family might be involved in this traffic. Among myosin proteins, myosin-X was a potential candidate for governing VE-Cad motions.

This unconventional motor protein is widely expressed in a variety of vertebrate tissues in particular in vascularized ones such as lung, heart, and placenta (6). Consistent with this observation, MyoX was recently found in the endothelium where it is involved in cell migration guidance (28). In different

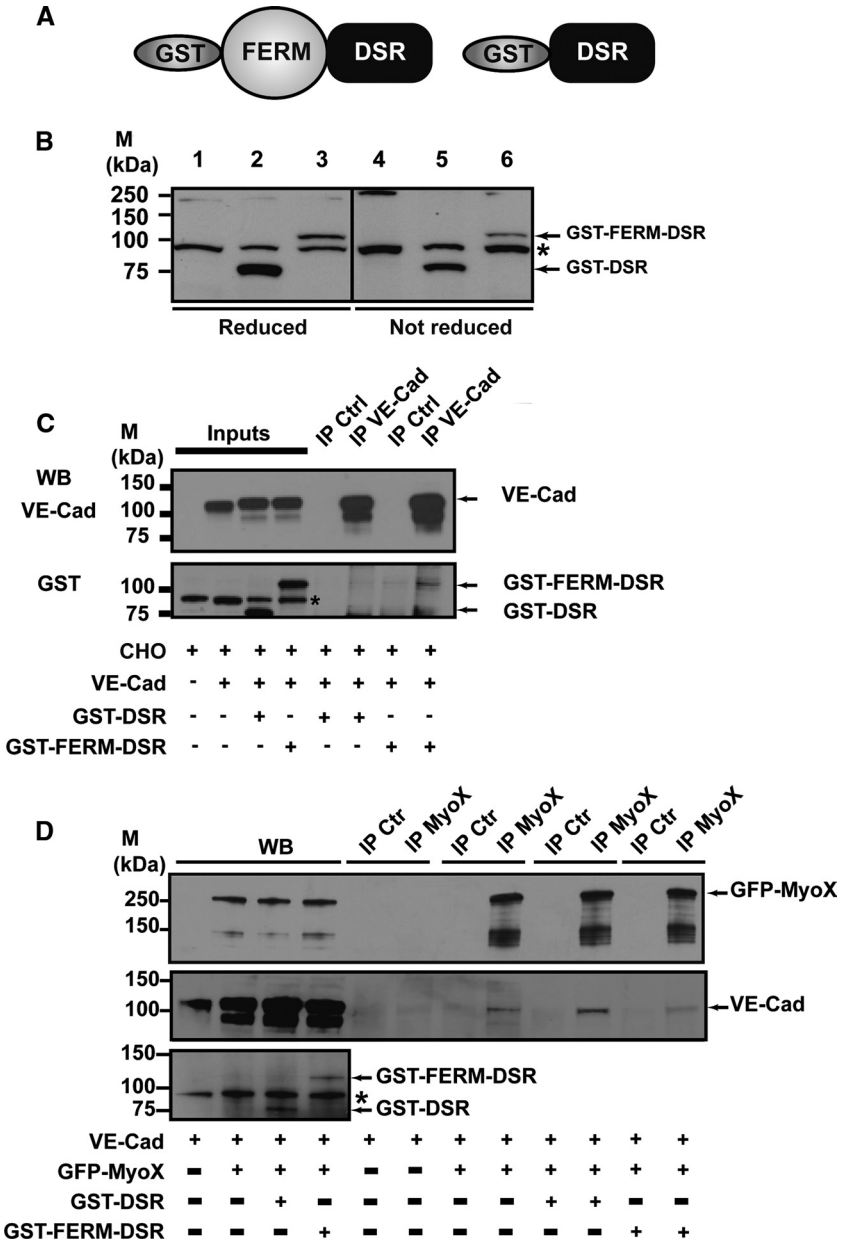

FIG. 13. Biochemical characterization of the recombinant proteins GST-FERM-DSR and GST-DSR. (A) Schematic representation of MyoX and its derived fragments. The recombinant fragment GST-FERM-DSR was designated to keep the capacity of MyoX to interact with VE-Cad via its FERM domain. The GST-DSR recombinant fragment was used as a control. (B) Expression of GST-DSR and GST-FERM-DSR. CHO cells were transfected with either GST-DSR (lanes 2 and 5) or GST-FERM-DSR (lanes 3 and 6) or not (lanes 1 and 4). Expression of GST-DSR and GST-FERM-DSR in CHO cells was verified by Western blotting (WB) using the anti-GST antibody. This antibody recognized an 80-kDa band and a 110-kDa band corresponding to GST-DSR and GST-FERM-DSR, respectively. Additionally, it also unspecifically recognized a protein present in CHO lysates (asterisk). (C) GST-FERM-DSR interacts with VE-cadherin. Anti-VE-Cad immunoprecipitations (IP VE-Cad) were performed on CHO cell lysates coexpressing either VE-Cad and GST-FERM-DSR or VE-Cad and GST-DSR using the Mab anti-VE-Cad BV9. As controls, aliquots of whole CHO lysates (inputs) and immunoprecipitations performd on CHO lysates using mouse nonimmune IgG (IP Ctrl) were analyzed in parallel. A 110-kDa band corresponding to GST-FERM-DSR was detected in the anti-VE-Cad immunoprecipitate, indicating that GST-FERM-DSR is able to interact with VE-Cad. The anti-GST antibody recognized, as in panel B, GST-DSR and GST-FERM-DSR, as well as an unspecific protein present in CHO cell lysates (asterisk). (D) Celluar VE-Cad sequestration by the MyoX FERM domain. VE-Cad-expressing CHO cells (40) were transiently transfected with plasmids coding for GFP-MyoX and either GST-DSR or GST-FERM-DSR. After cell lysis, anti-MyoX immunoprecipitations were resolved on 4 to 12% gradient gels, electrotransferred, and probed successively for VE-Cad, MyoX, and GST. As controls, aliquots of the various CHO lysates and immunoprecipitations performed using rabbit nonimmune IgG (IP Ctr) were analyzed in parallel. Molecular markers (M) are given at the left (B to D).

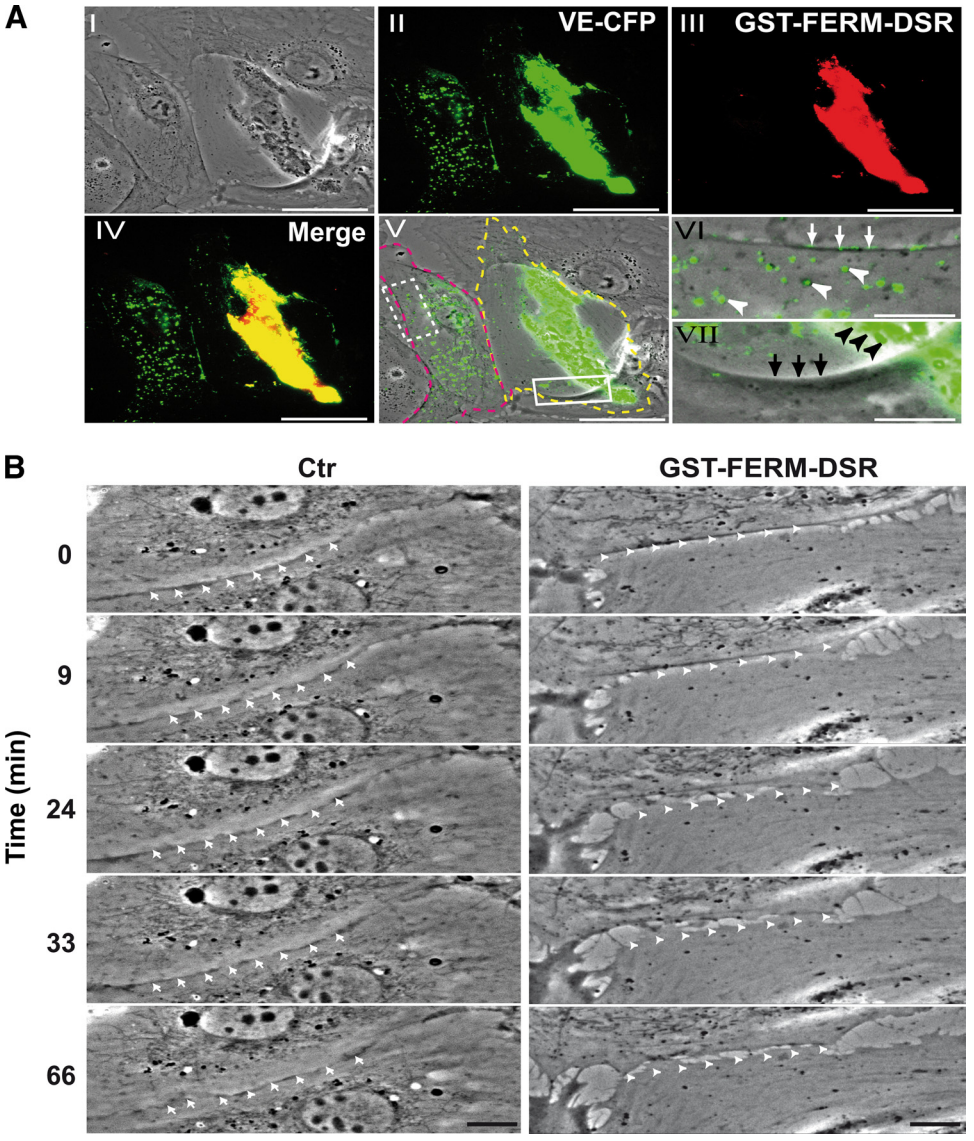

FIG. 14. Functional role of MyoX-mediated transport of VE-Cad. (A) Blockage of VE-CFP transport by GST-FERM-DSR expression. Subconfluent HUVECs transiently cotransfected with plasmids expressing VE-CFP and GST-FERM-DSR were observed 20 h posttransfection in phase-contrast (I) and in the cyan and red fluorescence channels. VE-CFP (II; green), GST-FERM-DSR (III; red), VE-CFP and GST-FERM-DSR merging (IV), and VE-CFP and phase-contrast merging (V, VI, and VII) allowed the visualization of two adjacent differentially-transfected cells: the cell at the right (delimited by the yellow dotted line) coexpressed GST-FERM-DSR and VE-CFP, while the cell at the left (delimited by pink dotted line) only expressed VE-CFP. Other cells of the fields are untransfected. The selected enlargements show that VE-CFP patches are at the cell-cell junctions (white arrows) and dispersed at the cell surface (white arrowheads) in the monotransfected cell (VI; dotted rectangle in V), whereas in the double-transfected cell, VE-CFP and GST-FERM-DSR colocalized and gathered around the cell nucleus (black arrowheads, VII; rectangle, V), indicating that GST-FERM-DSR blocked the VE-Cad transport to the cell edge. In control experiments, in cells coexpressing GST-DSR and VE-CFP, VE-CFP patches are located at cell-cell junctions (data not shown). Bars, 40 μm (I to V) and 10 μm (VI and VII). (B) Blockage of intercellular contact formation by GST-FERM-DSR expression. The sequences are selected from Movie S9 in the supplemental material and focus on the edges of two adjacent cells. In the right column, the cell below expressed GST-FERM-DSR, while the cell at the top is untransfected. In the left column, both cells expressed GST-DSR. Arrowheads show unstable junctions, whereas arrows point out stable junctions. Bars, 10 μm.

cell types, it is detected along the leading edge of lamellipodia (33) but, more frequently, at the tips of filopodia. In fact, MyoX is probably involved in the initiation of filopodium formation (9, 37). It moves along filopodial actin cables by an ATP-dependent walking mechanism toward the filament barbed ends, but also toward the cell body using the actin retrograde flow (5, 6, 26). MyoX possesses a FERM domain known to interact with the β-chains of integrins (43). Herein, we show that MyoX associates, via its FERM domain, with the VE-Cad–catenin complex (Fig. 9). This novel result underlines the versatility of MyoX FERM domain for interacting with different adhesive receptors.

We visualized the synchronous transit of MyoX and VE-Cad to or from the tips of filopodia. The forward movement that

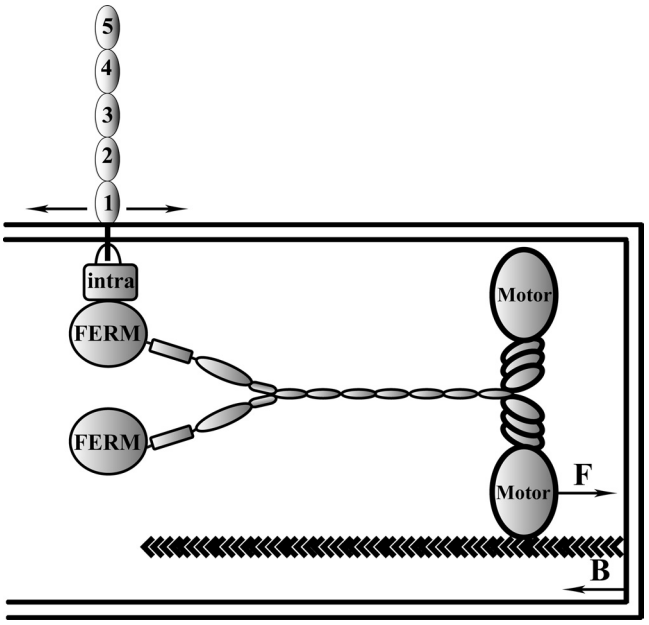

FIG. 15. Schematic model illustrating the movements of VE-Cad along filopodia (43). MyoX binds to actin filaments via its motor domain and to the VE-Cad–catenin complex (intra) via its FERM domain. Consequently, VE-Cad moves forward (F) toward the filopodium tip at a rate ranging around 700 nm s^{-1} and backwards (B) at a rate ranging around 30 nm s^{-1}.

reflects the barbed-end-directed movement of MyoX occurs at an average velocity of 700 nm s^{-1} (Fig. 11), a value similar to that reported in the literature (21). This is also consistent with the 500-nm s^{-1} rate of the recombinant MyoX head moving on actin filaments *in vitro* (20). This similitude between *in vivo* and *in vitro* velocities indicates that the rate of MyoX motion is not affected by the transport of cargoes as heavy as the VE-Cad–catenin complex. The backward movement exhibits a mean rate of 27 nm s^{-1} and allows the redistribution of VE-Cad at the cell body membrane. This motion is probably coupled to the continuous actin retrograde flow that causes the net transport of actin molecules within filaments from the plus end at the tip of a filopodium toward the minus end at the cell body. The speed of VE-Cad retrograde movement matches the speed for actin retrograde flow that is approximately 33 nm s^{-1} (32). Moreover, it could be noticed that the forward and backward movements are frequently interrupted by pausing events. They can be interpreted as the detaching of MyoX from actin cables or as the transient harpooning of either MyoX or its VE-Cad cargo by proteins in their close vicinity.

In Movie S10, we showed that cells sound their environment by emitting filopodia that propel VE-Cad molecules against neighboring cells. At these contact sites, VE-Cad elaborates homophilic interactions with VE-Cad partner molecules present in the counter membranes to constitute the first cell-cell anchor points. Subsequently, intercellular bridges between adjoining cells form and additional VE-Cad molecules transit on them prior to be engaged in their turn in homophilic interactions. VE-Cad accumulation thus reinforces the strength of these preliminary contacts.

VE-Cad molecules on their way back to the cell edges may be picked up again by other growing filopodia. These to-and-fro movements may adjust the local concentration of VE-Cad to the cell's needs in specific sites where cell-cell contacts are constructed or remodeled. Moreover, blockage of MyoX-mediated transport by a dominant-negative approach prevents the transportation of VE-Cad at the plasma membrane and subsequently inhibits formation of endothelial cell-cell contacts (Fig. 14A and B).

Once engaged in homophilic interactions, we frequently observed that VE-Cad moved along cortical actin fibers, thus assisting the lateral extension of cell-cell contacts (data not shown). At these more mature adhesion cell-cell contact sites, no colocalization of MyoX and VE-Cad was detected, suggesting that this motor protein is an effective partner for VE-Cad within filopodia but not in mature junctions (Fig. 8). This probably reflects the heterogeneity existing between the actin filaments inserted into filopodia and those decorating cell-cell junctions that form, in endothelial cells, a continuous thin belt (Fig. 5). This feature is in agreement with the existence of regioselective actin filament populations on which some myosins are recruited and other ones excluded (10).

MyoX-mediated accumulation of VE-Cad at filopodium tips is an important event probably involved in the restoration of endothelial monolayer integrity or in reclosure of wounds (see Movie S10 in the supplemental material). The multiplicity of cell-cell contacts created by filopodia that form bridges between adjacent cells seems to participate in the stabilization of nascent cell-cell junctions.

In conclusion, we have shown here that MyoX transports VE-Cad, an endothelium-specific cadherin to the tips of filopodia to promote homotypic cell-cell junction formation. A major goal for the future will be to examine whether this MyoX-supported transport of VE-Cad participates in the endothelium remodeling *in vivo*, in pathophysiological situations including endothelium repair or angiogenesis. In addition, it will be interesting to determine whether the concept of myosin-mediated transport of cadherins can be extended to tissues expressing other members of the cadherin family.

ACKNOWLEDGMENTS

We are indebted to the staff of the maternity ward from Hôpital Nord (Grenoble, France) for kindly collecting umbilical cords. The optical microscopy-cell imaging platform and the Institute Albert Bonniot are acknowledged for granting access to the confocal microscopy facilities and help with image acquisition and analysis. We thank R. E. Cheney for GFP–myoxin-X, R.-M. Mège, and R. Y. Tsien for DSRed cDNA constructs and L. Blanchoin for helpful discussions.

This work was supported by the Ligue Régionale de Savoie Contre le Cancer, the Agence Nationale de la Recherche (ANR, PCV), and the Association pour la Recherche sur le Cancer (grants 4447 and 3775). S.A. was a recipient of fellowships from the Commissariat à l'Energie Atomique (CEA) and the Agence Nationale de Recherche. A.C.-P., S.H., and M.D. are recipients of fellowships from the CEA, the Association de Recherche sur la Polyarthrite, and the Agence Nationale de Recherche (ANR-06-PCV), respectively.

REFERENCES

1. **Aberle, H., A. Bauer, J. Stappert, A. Kispert, and R. Kemler.** 1997. Beta-catenin is a target for the ubiquitin-proteasome pathway. EMBO J. **16:**3797–3804.
2. **Adams, C. L., Y. T. Chen, S. J. Smith, and W. J. Nelson.** 1998. Mechanisms of epithelial cell-cell adhesion and cell compaction revealed by high-resolution tracking of E-cadherin-green fluorescent protein. J. Cell Biol. **142:**1105–1119.

3. **Adams, C. L., W. J. Nelson, and S. J. Smith.** 1996. Quantitative analysis of cadherin-catenin-actin reorganization during development of cell-cell adhesion. J. Cell Biol. **135:**1899–1911.
4. **Bear, J. E., and F. B. Gertler.** 2009. Ena/VASP: towards resolving a pointed controversy at the barbed end. J. Cell Sci. **122:**1947–1953.
5. **Berg, J. S., and R. E. Cheney.** 2002. Myosin-X is an unconventional myosin that undergoes intrafilopodial motility. Nat. Cell Biol. **4:**246–250.
6. **Berg, J. S., B. H. Derfler, C. M. Pennisi, D. P. Corey, and R. E. Cheney.** 2000. Myosin-X, a novel myosin with pleckstrin homology domains, associates with regions of dynamic actin. J. Cell Sci. **113:**3439–3451.
7. **Block, J., T. E. Stradal, J. Hanisch, R. Geffers, S. A. Kostler, E. Urban, J. V. Small, K. Rottner, and J. Faix.** 2008. Filopodia formation induced by active mDia2/Drf3. J. Microsc. **231:**506–517.
8. **Bogatcheva, N. V., and A. D. Verin.** 2008. The role of cytoskeleton in the regulation of vascular endothelial barrier function. Microvasc. Res. **76:**202–207.
9. **Bohil, A. B., B. W. Robertson, and R. E. Cheney.** 2006. Myosin-X is a molecular motor that functions in filopodia formation. Proc. Natl. Acad. Sci. U. S. A. **103:**12411–12416.
10. **Brawley, C. M., and R. S. Rock.** 2009. Unconventional myosin traffic in cells reveals a selective actin cytoskeleton. Proc. Natl. Acad. Sci. U. S. A. **106:** 9685–9690.
11. **Breviario, F., L. Caveda, M. Corada, I. Martin-Padura, P. Navarro, J. Golay, M. Introna, D. Gulino, M. G. Lampugnani, and E. Dejana.** 1995. Functional properties of human vascular endothelial cadherin (7B4/cadherin-5), an endothelium-specific cadherin. Arterioscler. Thromb. Vasc. Biol. **15:**1229–1239.
12. **Campbell, R. E., O. Tour, A. E. Palmer, P. A. Steinbach, G. S. Baird, D. A. Zacharias, and R. Y. Tsien.** 2002. A monomeric red fluorescent protein. Proc. Natl. Acad. Sci. U. S. A. **99:**7877–7882.
13. **Coue, M., S. L. Brenner, I. Spector, and E. D. Korn.** 1987. Inhibition of actin polymerization by latrunculin A. FEBS Lett. **213:**316–318.
14. **Erdbruegger, U., M. Haubitz, and A. Woywodt.** 2006. Circulating endothelial cells: a novel marker of endothelial damage. Clin. Chim. Acta **373:**17–26.
15. **Faix, J., D. Breitsprecher, T. E. Stradal, and K. Rottner.** 2009. Filopodia: complex models for simple rods. Int. J. Biochem. Cell Biol. **41:**1656–1664.
16. **Gulino, D., E. Delachanal, E. Concord, Y. Genoux, B. Morand, M. O. Valiron, E. Sulpice, R. Scaife, M. Alemany, and T. Vernet.** 1998. Alteration of endothelial cell monolayer integrity triggers resynthesis of vascular endothelium cadherin. J. Biol. Chem. **273:**29786–29793.
17. **Gupton, S. L., and F. B. Gertler.** 2007. Filopodia: the fingers that do the walking. Sci. STKE **2007:**re5.
18. **Hermant, B., S. Bibert, E. Concord, B. Dublet, M. Weidenhaupt, T. Vernet, and D. Gulino-Debrac.** 2003. Identification of proteases involved in the proteolysis of vascular endothelium cadherin during neutrophil transmigration. J. Biol. Chem. **278:**14002–14012.
19. **Heyraud, S., M. Jaquinod, C. Durmort, E. Dambroise, E. Concord, J. P. Schaal, P. Huber, and D. Gulino-Debrac.** 2008. Contribution of annexin 2 to the architecture of mature endothelial adherens junctions. Mol. Cell. Biol. **28:**1657–1668.
20. **Homma, K., J. Saito, R. Ikebe, and M. Ikebe.** 2001. Motor function and regulation of myosin X. J. Biol. Chem. **276:**34348–34354.
21. **Kerber, M. L., D. T. Jacobs, L. Campagnola, B. D. Dunn, T. Yin, A. D. Sousa, O. A. Quintero, and R. E. Cheney.** 2009. A novel form of motility in filopodia revealed by imaging myosin-X at the single-molecule level. Curr. Biol. **19:** 967–973.
22. **Lampugnani, M. G., M. Resnati, M. Raiteri, R. Pigott, A. Pisacane, G. Houen, L. P. Ruco, and E. Dejana.** 1992. A novel endothelial-specific membrane protein is a marker of cell-cell contacts. J. Cell Biol. **118:**1511–1522.
23. **Maddugoda, M. P., M. S. Crampton, A. M. Shewan, and A. S. Yap.** 2007. Myosin VI and vinculin cooperate during the morphogenesis of cadherin cell cell contacts in mammalian epithelial cells. J. Cell Biol. **178:**529–540.
24. **Mallavarapu, A., and T. Mitchison.** 1999. Regulated actin cytoskeleton assembly at filopodium tips controls their extension and retraction. J. Cell Biol. **146:**1097–1106.
25. **Martel, V., L. Vignoud, S. Dupe, P. Frachet, M. R. Block, and C. Albiges-Rizo.** 2000. Talin controls the exit of the integrin alpha 5 beta 1 from an early compartment of the secretory pathway. J. Cell Sci. **113:**1951–1961.
26. **Mattila, P. K., and P. Lappalainen.** 2008. Filopodia: molecular architecture and cellular functions. Nat. Rev. Mol. Cell Biol. **9:**446–454.
27. **Mege, R. M., J. Gavard, and M. Lambert.** 2006. Regulation of cell-cell junctions by the cytoskeleton. Curr. Opin. Cell Biol. **18:**541–548.
28. **Pi, X., R. Ren, R. Kelley, C. Zhang, M. Moser, A. B. Bohil, M. Divito, R. E. Cheney, and C. Patterson.** 2007. Sequential roles for myosin-X in BMP6-dependent filopodial extension, migration, and activation of BMP receptors. J. Cell Biol. **179:**1569–1582.
29. **Pollard, T. D.** 2007. Regulation of actin filament assembly by Arp2/3 complex and formins. Annu. Rev. Biophys. Biomol. Struct. **36:**451–477.
30. **Raich, W. B., C. Agbunag, and J. Hardin.** 1999. Rapid epithelial-sheet sealing in the Caenorhabditis elegans embryo requires cadherin-dependent filopodial priming. Curr. Biol. **9:**1139–1146.
31. **Rudini, N., and E. Dejana.** 2008. Adherens junctions. Curr. Biol. **18:**R1080–R1082.
32. **Schelhaas, M., H. Ewers, M. L. Rajamaki, P. M. Day, J. T. Schiller, and A. Helenius.** 2008. Human papillomavirus type 16 entry: retrograde cell surface transport along actin-rich protrusions. PLoS Pathog. **4:**e1000148.
33. **Sousa, A. D., J. S. Berg, B. W. Robertson, R. B. Meeker, and R. E. Cheney.** 2006. Myo10 in brain: developmental regulation, identification of a headless isoform and dynamics in neurons. J. Cell Sci. **119:**184–194.
34. **Svitkina, T. M., E. A. Bulanova, O. Y. Chaga, D. M. Vignjevic, S. Kojima, J. M. Vasiliev, and G. G. Borisy.** 2003. Mechanism of filopodia initiation by reorganization of a dendritic network. J. Cell Biol. **160:**409–421.
35. **Tesfamariam, B., and A. F. DeFelice.** 2007. Endothelial injury in the initiation and progression of vascular disorders. Vascul. Pharmacol. **46:**229–237.
36. **Tokuo, H., and M. Ikebe.** 2004. Myosin X transports Mena/VASP to the tip of filopodia. Biochem. Biophys. Res. Commun. **319:**214–220.
37. **Tokuo, H., K. Mabuchi, and M. Ikebe.** 2007. The motor activity of myosin-X promotes actin fiber convergence at the cell periphery to initiate filopodia formation. J. Cell Biol. **179:**229–238.
38. **Vasioukhin, V., C. Bauer, M. Yin, and E. Fuchs.** 2000. Directed actin polymerization is the driving force for epithelial cell-cell adhesion. Cell **100:**209–219.
39. **Vasioukhin, V., and E. Fuchs.** 2001. Actin dynamics and cell-cell adhesion in epithelia. Curr. Opin. Cell Biol. **13:**76–84.
40. **Wallez, Y., F. Cand, F. Cruzalegui, C. Wernstedt, S. Souchelnytskyi, I. Vilgrain, and P. Huber.** 2007. Src kinase phosphorylates vascular endothelial-cadherin in response to vascular endothelial growth factor: identification of tyrosine 685 as the unique target site. Oncogene **26:**1067–1077.
41. **Waschke, J., F. E. Curry, R. H. Adamson, and D. Drenckhahn.** 2005. Regulation of actin dynamics is critical for endothelial barrier functions. Am. J. Physiol. Heart Circ. Physiol. **288:**H1296–H1305.
42. **Wood, W., and P. Martin.** 2002. Structures in focus—filopodia. Int. J. Biochem. Cell Biol. **34:**726–730.
43. **Zhang, H., J. S. Berg, Z. Li, Y. Wang, P. Lang, A. D. Sousa, A. Bhaskar, R. E. Cheney, and S. Stromblad.** 2004. Myosin-X provides a motor-based link between integrins and the cytoskeleton. Nat. Cell Biol. **6:**523–531.